Basic phenomenology for heavy-ion collisions: Lecture I

Wojciech Florkowski[1,2]

[1] Jan Kochanowski University, Kielce, Poland
[2] Institute of Nuclear Physics, Polish Academy of Sciences, Kraków, Poland

Cracow School of Theoretical Physics, LIV Course, 2014
QCD meets experiment, June 12–20, 2014

Outline

LECTURE I

Outline

LECTURE II

Outline

LECTURE III

STANDARD MODEL (MODULES) of HEAVY–ION COLLISIONS

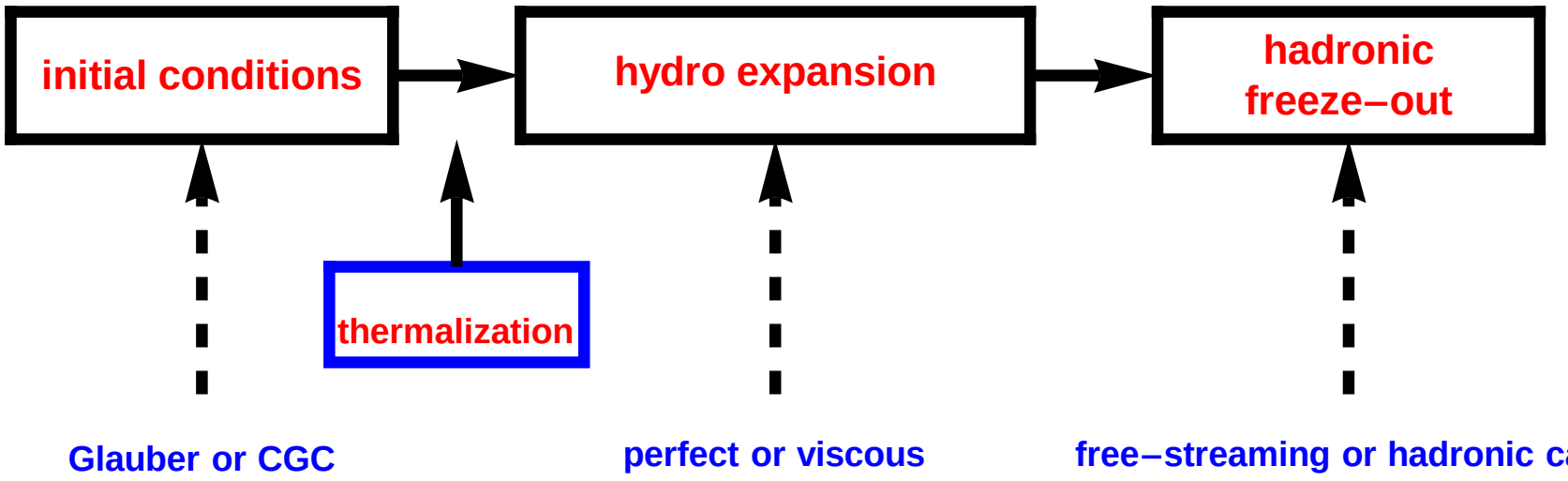

NEW: FLUCTUATIONS IN THE INITIAL STATE / EVENT–BY–EVENT HYDRO / FINAL–STATE FLUCTUATIONS

EQUATION OF STATE?

VISCOSITY?

Early-time physics/conditions – Y. Kovchegov, L. McLerran
Thermalization – F. Gelis, P. Braun-Munzinger
Hydrodynamics - P. Bozek, M. Strickland
Phase transition - M. Gaździcki, Ch. Hoelbling
Freeze-out (as seen by correlations) - A. Kisiel

1. INTRODUCTION

1.1 High-energy nuclear collisions

Physics of the ultra-relativistic heavy-ion collisions is an **interdisciplinary field** which connects the **high-energy physics of elementary particles** with the **nuclear physics**. There exist also connections to **astrophysics** and **cosmology**.

The name **"heavy-ions"** is used for heavy atomic nuclei, whereas the term **"ultra-relativistic energy"** denotes the energy regime where the kinetic energy exceeds significantly the rest energy (I use natural units where $c = \hbar = k_B = 1$).

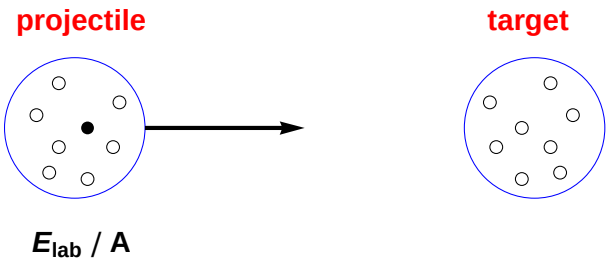

$$E_{\rm lab}/A \gg m_{\rm N} \sim 1 \text{ GeV}. \quad (1)$$

$E_{\rm lab}$ – energy in the lab, A – atomic number, $m_{\rm N}$ – nucleon mass.

In the case of colliders, we speak more often about the energy in the center-of-mass frame per nucleon pair.

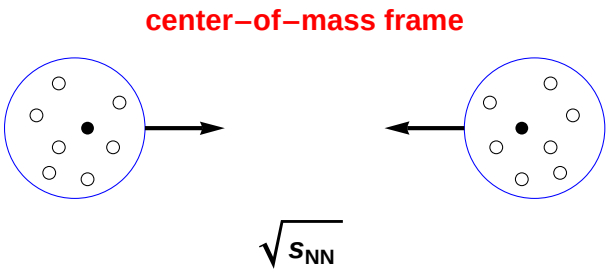

$$\sqrt{s_{\rm NN}} \gg m_{\rm N} \sim 1 \text{ GeV}. \quad (2)$$

1.1 High-energy nuclear collisions

The first experiments with the ultra-relativistic heavy ions (with energies exceeding 10 GeV per nucleon in the projectile beam) took place at the **Brookhaven National Laboratory (BNL)** and at the **European Organization for Nuclear Research (CERN)** in **1986**.

The **Alternating Gradient Synchrotron (AGS)** at BNL accelerated beams up to ^{28}Si at 14 GeV per nucleon.

At CERN, the **Super Proton Synchrotron (SPS)** accelerated ^{16}O at 60 and 200 GeV per nucleon in 1986, and ^{32}S at 200 GeV per nucleon in 1987.

In 1990 a long-term project on heavy-ion physics was realized at CERN with several weeks of ^{32}S beams. In the spring of 1992 the experiments with ^{197}Au beams at 11 GeV per nucleon were initiated at BNL.

In 1995 the completely new experiments took place at CERN with ^{208}Pb beams at 158 GeV per nucleon. These were for the first time really ultra-relativistic "heavy" ions providing large volumes and lifetimes of the reaction zone.

1.1 High-energy nuclear collisions

In 2000 the first data from the **Relativistic Heavy Ion Collider (RHIC)** at BNL were collected. During the first run, the maximum energy of 130 GeV per nucleon pair was achieved. In the next years new runs took place with the maximum energy of 200 GeV per nucleon pair. One of those runs was devoted to the study of the deuteron-gold collisions which were analyzed in order to get the proper reference point for the more complicated gold on gold collisions.

Satellite view of RHIC and BNL (Long Island, New York, USA).

1.1 High-energy nuclear collisions

The main activity in the field is connected now with **Large Hadron Collider (LHC)** at CERN (Pb on Pb reactions at $\sqrt{s_{\mathrm{NN}}}$ = 2.76 TeV, start Nov.-Dec., 2010).

Aerial view of CERN and Geneva (Switzerland).

Nevertheless, the performance of new experiments at lower energies is also very important, since this allows us to study the energy dependence of many characteristics of the particle production, and direct searches for new phenomena, **NA61** at CERN, **STAR** at BNL.

1.2 Theoretical methods

In the ultra-relativistic heavy-ion collisions very large numbers of particles are produced (we deal with so called large particle **multiplicities**).

For example, in the central Au+Au collisions at RHIC, at the highest beam energy $\sqrt{s_{\mathrm{NN}}}$ = 200 GeV, the total charged particle multiplicity is about 5000. Hence, the number of produced particles exceeds the number of initial nucleons by a factor of 10.

In this situation, different theoretical methods are used, which are suitable for description of large macroscopic systems, e.g., **thermodynamics, hydrodynamics, kinetic (transport) theory, field theory at finite temperature and density, non-equilibrium field theory, Monte-Carlo simulations**.

... we also know the underlying fundamental theory!

1.3 Quantum Chromodynamics

In high-energy nuclear collisions a **many-body system of strongly interacting particles is produced**. The fundamental theory of the strong interactions is **Quantum Chromodynamics** (QCD), the theory of quarks and gluons which are confined in hadrons, i.e., baryons and mesons.

A few historical steps:

1963 – proposal of Gell-Mann and Zweig suggesting that the structure of hadrons could be explained by the existence of smaller particles inside hadrons.

In 1964 Greenberg and in 1965 Han with Nambu proposed that quarks possessed an additional degree of freedom, that was later called the **color charge**. Han and Nambu noted that quarks might interact via exchanges of an octet of vector gauge bosons (later **gluons**).

1.3 Quantum Chromodynamics: asymptotic freedom

Feynman and Bjorken argued that high-energy experiments should reveal the existence of partons, i.e., particles that are parts of hadrons, suggestions spectacularly verified in the **deep inelastic scattering** of electrons on protons, the experiments carried out at the Stanford Linear Accelerator Center (SLAC) in 1969. The partons were identified with quarks.

1973 – the discovery of **asymptotic freedom** in the strong interactions by Gross, Politzer, and Wilczek allowed for making precise predictions of the results of many high-energy experiments in the framework of the perturbative quantum field theory — the asymptotic freedom is the property that the **interaction between particles becomes weaker at shorter distances**.

1975 – Collins and Perry argued that “superdense matter (found in neutron-star cores, exploding black holes, and the early big-bang universe) consists of quarks rather than of hadrons”.

1.3 Quantum Chromodynamics

1975 – Cabibbo and Parisi identified the limiting Hagedorn temperature with the temperature of the phase transition from hadronic to quark matter, they also sketched the first phase diagram of strongly interacting matter.

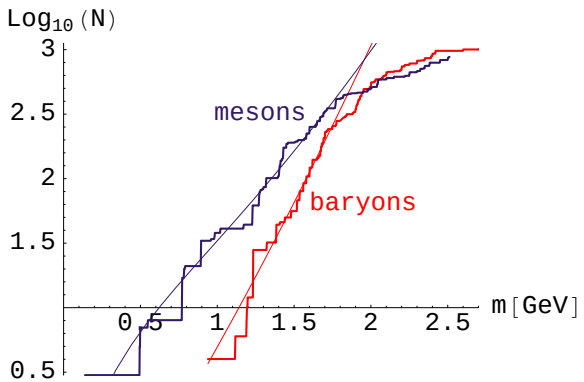

Hadron mass spectrum grows like e^{m/T_H} where T_H is the Hagedorn temperature, in this case there is a limiting temperature for hadrons, integrals over m of the expressions such as $e^{m/T_H - \sqrt{m^2+p^2}/T}$ diverge if $T \geq T_H$!

W. Broniowski and WF, different T_H for baryons and mesons (see figure)

$T \to \infty$, density grows like T^3, inter-particle distance $\sim 1/T \to 0$, weakly interacting system!

Gauge theories at finite temperature:
Kislinger and Morley (1975), Freedman and McLerran (1976),
Shuryak, who in 1978 introduced the name **quark-gluon plasma (QGP)**,
Kapusta (1979), ...

1.3 Quantum Chromodynamics: confinement

Probably the most striking feature of QCD is the **color confinement**, which is the other side of the asymptotic freedom. This is the phenomenon that color charged particles (such as quarks and gluons) cannot be isolated as separate objects. In other words, quarks and gluons cannot be directly observed. The physical concept of confinement may be illustrated by a string which is spanned between the quarks when we try to separate them. If the quarks are pulled apart too far, large energy is deposited in the string which breaks into smaller pieces.

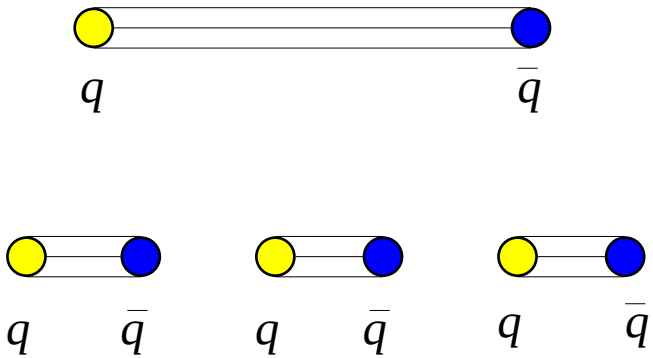

1.4 Quark-gluon plasma

The main challenge of the ultra-relativistic heavy-ion collisions is the observation of the two phase transitions predicted by QCD, i.e., the **deconfinement** and **chiral phase transitions**.

As we have mentioned above, at Earth conditions (i.e., at low energy densities) quarks and gluons are confined in hadrons. However, **with increasing temperature (heating) and/or increasing baryon density (compression), a phase transition may occur to the state where the ordinary hadrons do not exist anymore; quarks and gluons become the proper degrees of freedom, and their motion is not confined to hadrons**.

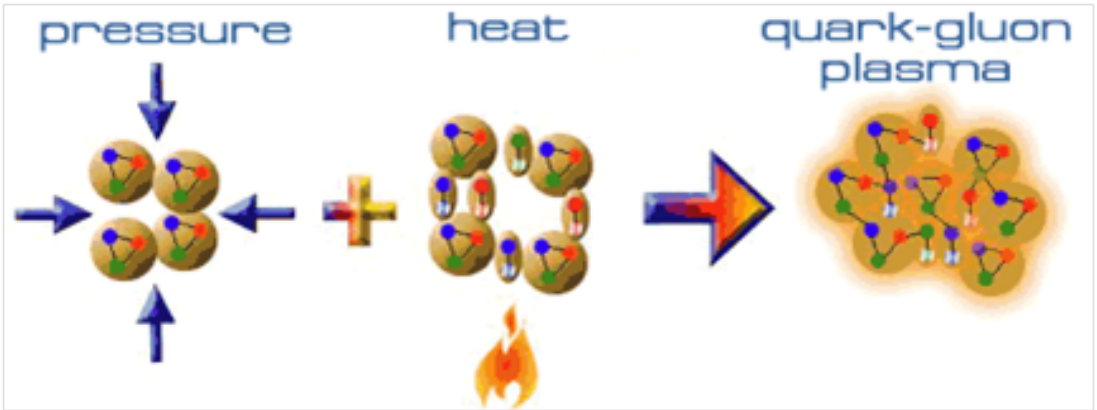

direct searches for the phase transition by studying the energy dependence of physical observables discussed in Marek Gaździcki's lectures

1.4 Quark-gluon plasma

Two concepts:

1) Notion based on the asymptotic freedom — QGP as an asymptotic state available at extremely high energies

2) Phenomenological approach — QGP as a new state of strongly interacting matter, whose properties can be inferred from experimental and theoretical investigations carried out at the presently available energies (a new phase consisting of quarks and gluons, locally equilibrated, with small viscosity,...)

1.4 Quark-gluon plasma: equation of state

massless gluons (Stefan-Boltzmann's law)

$$\varepsilon_g = 16\,\frac{\pi^2}{30}\,T^4, \qquad P_g = \frac{1}{3}\,\varepsilon_g$$

massless quarks

$$\varepsilon_q + \varepsilon_{\overline{q}} = 6N_f\left(\frac{7\pi^2}{120}\,T^4 + \frac{1}{4}\,\mu^2 T^2 + \frac{1}{8\pi^2}\,\mu^4\right),$$

$$P_q + P_{\overline{q}} = \frac{1}{3}\left(\varepsilon_q + \varepsilon_{\overline{q}}\right)$$

μ is one third of the baryon chemical potential μ_B, $\mu = \frac{1}{3}\mu_B$
WEAKLY INTERACTING GAS of quarks and gluons, B – bag constant

$$\varepsilon_{\rm qgp} = \varepsilon_g(T) + \varepsilon_q(T,\mu) + \varepsilon_{\overline{q}}(T,\mu) + B$$

or

$$P_{\rm qgp} = P_g(T) + P_q(T,\mu) + P_{\overline{q}}(T,\mu) - B$$

1.4 Quark-gluon plasma: naive phase transition

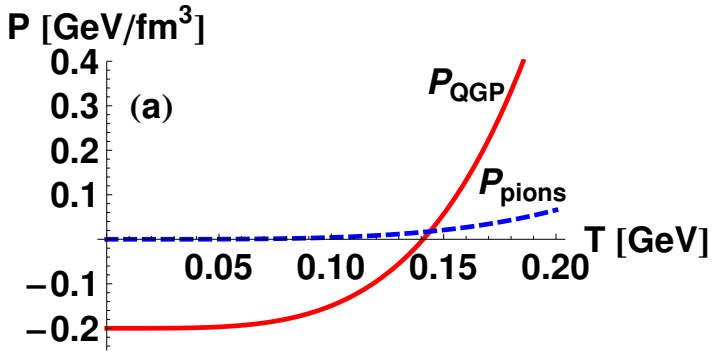

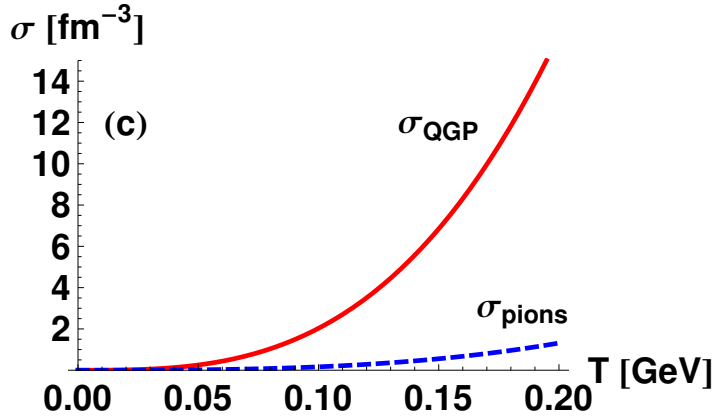

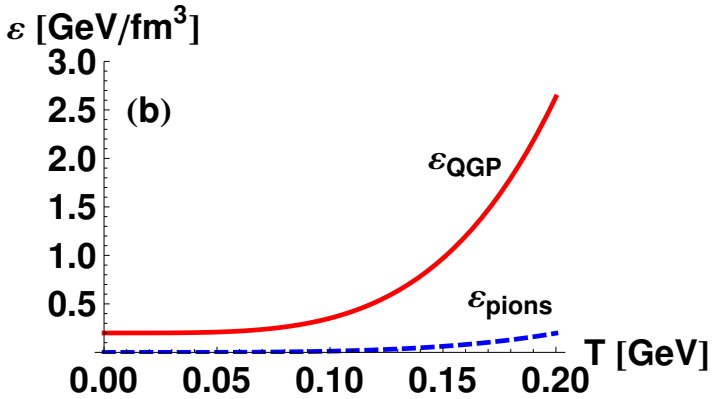

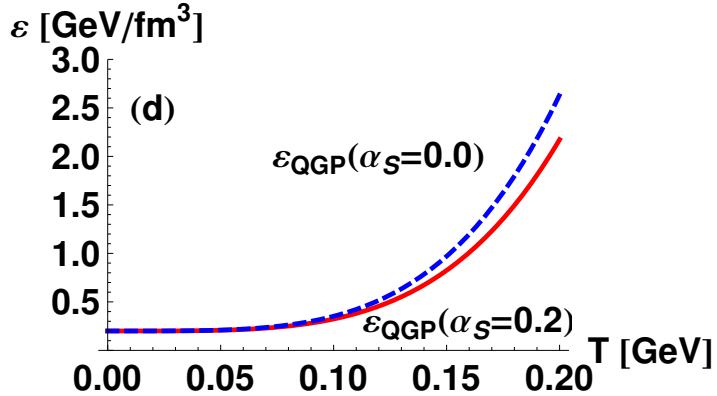

first order phase transition between a weakly interacting plasma and a pion gas

1.4 Quark-gluon plasma: lattice QCD simulations

Calculations done at zero baryon chemical potential, $\mu_B = 0$!
sound velocity $c_s^2(T) = \frac{\partial P}{\partial \varepsilon}$
drops to zero at the first order phase transition
stays large at the **crossover phase transition**

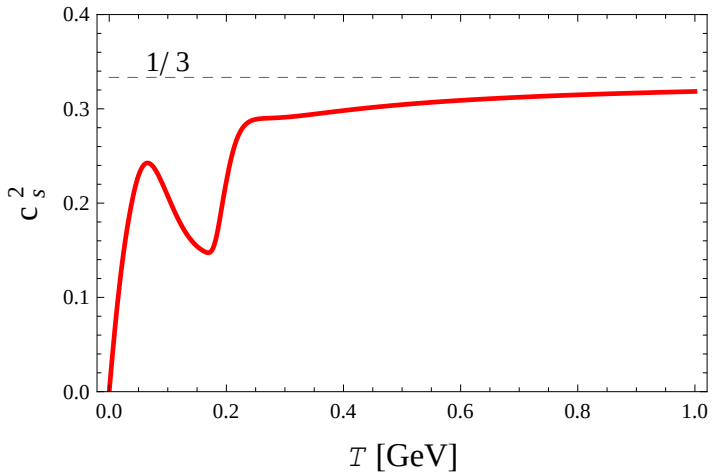

lattice simulations of QCD done by the Budapest-Wuppertal group (Z. Fodor et al.),
figure – connecting hadron-resonance gas with LQCD by M. Chojnacki and WF (2007)

1.4 Quark-gluon plasma: phase diagram

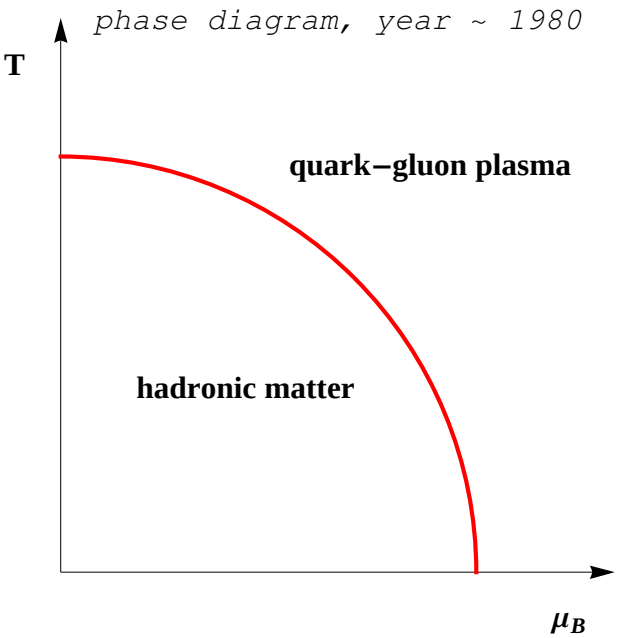

Cabibbo-Parisi

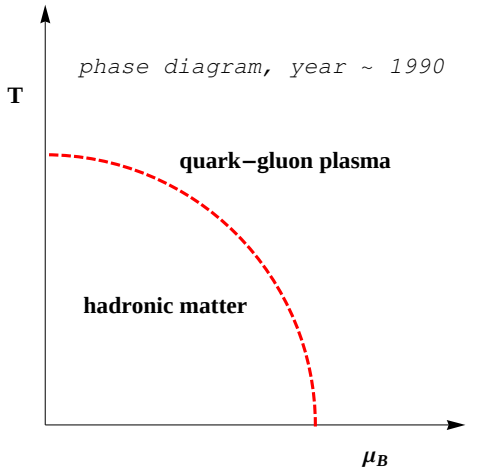

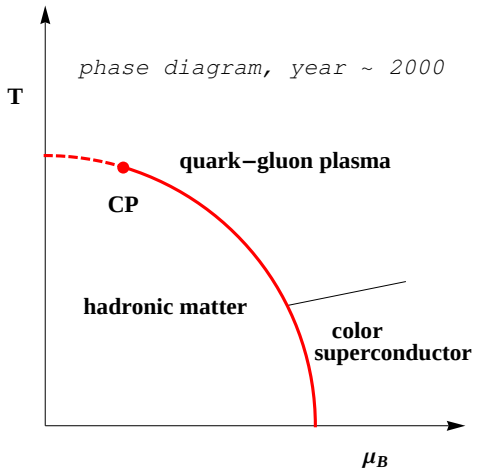

1.5 Chiral symmetry

In the limit of vanishing masses the left- and right-handed quarks become decoupled from each other and QCD becomes invariant under their interchange — left- and right-handed quark currents are separately conserved, each state of the theory should have a degenerate partner of the opposite parity. On the other hand, we know that hadrons have well defined parity, and no such parity partners are observed!

The paradox is resolved by the phenomenon of the **spontaneous breakdown of chiral symmetry**: the chiral symmetry of the interaction is broken by the true ground state of the theory, Nambu (1961) in the context of Nambu–Jona-Lasinio model.

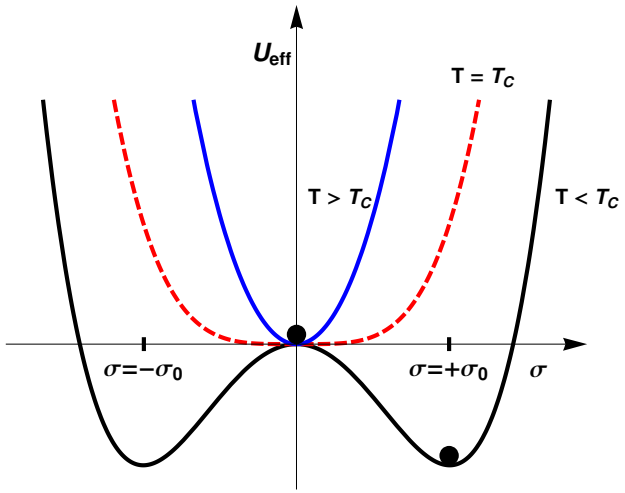

Quark condensate, $\langle\bar{\psi}\psi\rangle$, is the order parameter of the chiral phase transition, drops to zero above T_c.

1.6 Hot and dense nuclear matter

Heavy-ion collisions are the only way to compress and heat up nuclear matter in laboratory conditions.

The particles inside such a system do not propagate completely freely: their Compton wavelength may be comparable with their mean free path. In this situation, we expect that some of the particle properties (e.g., hadron masses, widths or coupling constants) can be changed. These **in-medium modifications** can lead to the experimentally observed phenomena.

For example, the change of the ρ meson mass and/or width in dense matter can influence the measured dilepton spectrum. Nowadays, one attempts to connect in-medium modifications of hadron properties with the **partial restoration of chiral symmetry**.

Gell-Mann–Oakes-Renner relation,

$$f_\pi^2 m_\pi^2 = m_q \langle \bar{\psi}\psi \rangle \ .$$

2. BASIC DICTIONARY

2.1 Participants, spectators, and impact parameter

At very high energies, simple geometric concepts are often used, for example, one separates so called participants from spectators — if we assume that all nucleons propagate along parallel, straight line trajectories, then the nucleons which do not meet any other nucleons on their way are called **spectators**. Other nucleons which interact with each other are called **participants**.

The participants which suffered at least one inelastic collision are called the **wounded nucleons**.

A two-dimensional vector connecting centers of the colliding nuclei in the plane transverse to the nucleon trajectories is called the **impact vector**, and its length is the **impact parameter**.

In particle as well as in nuclear physics it is practical to introduce a coordinate system, where the spatial z-axis is parallel to the beam of the accelerator, and where the **impact vector b** points in x-direction. The two axes, x and z, span the **reaction plane** of a given collision.

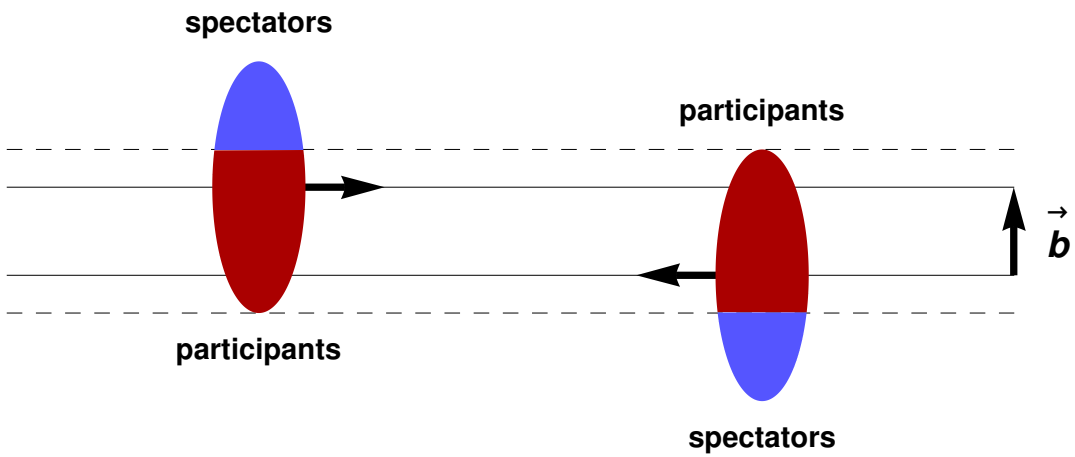

2.1 Participants, spectators, and impact parameter

The very important class of **central collisions** corresponds to the zero impact parameter (in practice one considers a group of events which are characterized by the smallest values of the impact parameter).

The measurements averaged over different impact parameters are called the **minimum-bias** data. The value of the impact parameter determines the number of the participants, N_{part}, as well as the number of the spectators, N_{spec}. An estimate of N_{part} allows us to compare proton-nucleus (pA) and nucleus-nucleus (AA) results to pp data by means of a simple rescaling (there are obviously two participating nucleons in a pp collision).

Experimentally, the value of N_{spec} may be inferred from the measurement of the energy deposited in the **zero-degree calorimeter** or in the **veto calorimeter**.

2.2.1 Kinematical variables: transverse mass

The component of a three-vector **A** parallel to z-axis is usually denoted by $\mathbf{A}_{\parallel}$, and the transverse component is $\mathbf{A}_{\perp} = \mathbf{A} - \mathbf{A}_{\parallel}$. The **transverse mass** of a particle is defined as

$$m_{\perp} = \sqrt{m^2 + \mathbf{p}_{\perp}^2}, \tag{3}$$

where m and **p** are the particle's mass and three-momentum [1].

The measured $m_{\perp}$-distribution of the produced particles is typically of the **exponential form** (for not too large transverse momenta, $p_{\perp} < 1$–2 GeV)

$$\frac{dN}{2\pi\, m_{\perp}\, dm_{\perp}} = A \exp\left(-m_{\perp}/\lambda\right). \tag{4}$$

The two parameters A and λ are obtained from the fits to the experimental data.

[1] The "transverse" quantities are sometimes denoted by the subscript T, e.g., m_T or p_T. The "longitudinal" quantities are then denoted by the subscript L, e.g., p_L.

2.2.1 Kinematical variables: transverse mass

The measurements done by the NA49 Collaboration at CERN. The transverse-mass spectra of π^-, K^+, and K^- at midrapidity ($|y| < 0.1$ for kaons and $0 < y < 0.2$ for pions) in the central Pb+Pb collisions at the energy $E_{\rm lab} = 40$ A GeV (triangles), 80 A GeV (squares), and 158 A GeV (circles). The lines are the exponential fits to the spectra in the interval 0.2 GeV $< m_T - m <$ 0.7 GeV. The values for 80 A GeV and 158 A GeV are rescaled by the factors of 10 and 100, respectively.

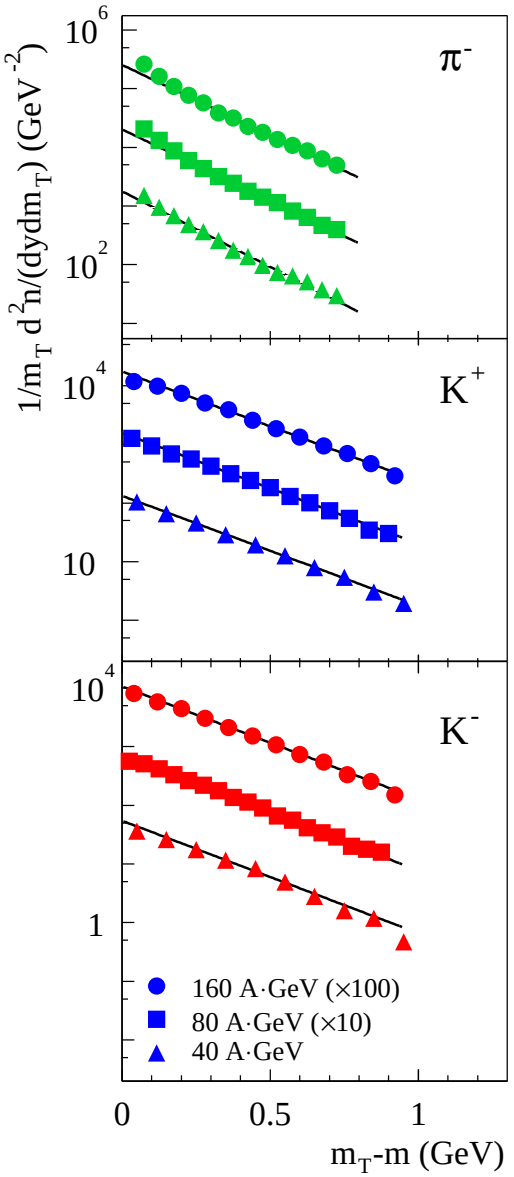

2.2.2 Kinematical variables: rapidity

Since we deal with relativistic energies, it is useful to use the **rapidity** instead of the standard velocity

$$\mathrm{y} = \frac{1}{2} \ln \frac{(E+p_{\parallel})}{(E-p_{\parallel})} = \operatorname{arctanh}\left(\frac{p_{\parallel}}{E}\right) = \operatorname{arctanh}\left(\mathrm{v}_{\parallel}\right). \tag{5}$$

Here E is the energy of a particle, $E = \sqrt{m^2 + \mathbf{p}^2}$, and $\mathrm{v}_{\parallel} = p_{\parallel}/E$ is the longitudinal component of the velocity. **Rapidity is additive under Lorentz boosts along the z-axis.**

Using the rapidity and the transverse mass, we can calculate the energy and the longitudinal momentum of a particle from the equations

$$E = p^0 = m_{\perp} \cosh \mathrm{y} \tag{6}$$

and

$$p_{\parallel} = m_{\perp} \sinh \mathrm{y}. \tag{7}$$

2.2.2 Kinematical variables: rapidity

The measurements done by the NA49 Collaboration at CERN. The rapidity distributions of π^-, K^+, and K^- in the central Pb+Pb collisions at the energy $E_{\rm lab} = 40$ A GeV, 80 A GeV, and 158 A GeV. The closed symbols indicate the measured points, whereas the open points are reflection of the measured points with respect to the axis $y = 0$.

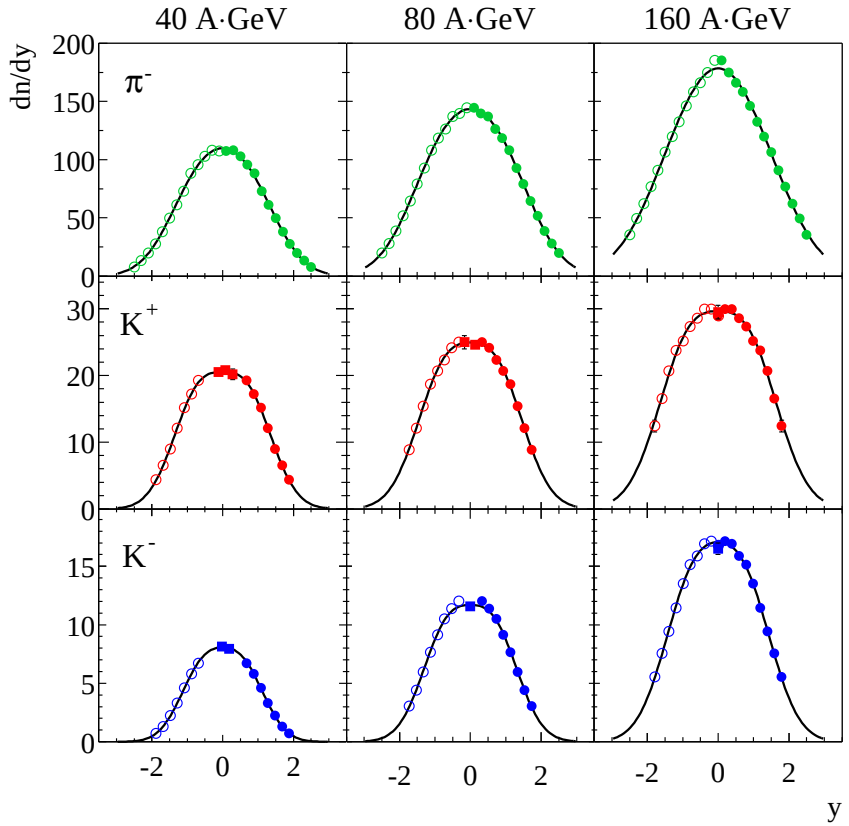

2.2.2 Kinematical variables: rapidity

The measurement of the BRAHMS Collaboration at BNL (Au+Au collisions at $\sqrt{s_{\rm NN}} = 200$ GeV, the most central events). Rapidity distributions **(a)** and average transverse momenta **(b)** of charged pions, charged kaons, protons and antiprotons.

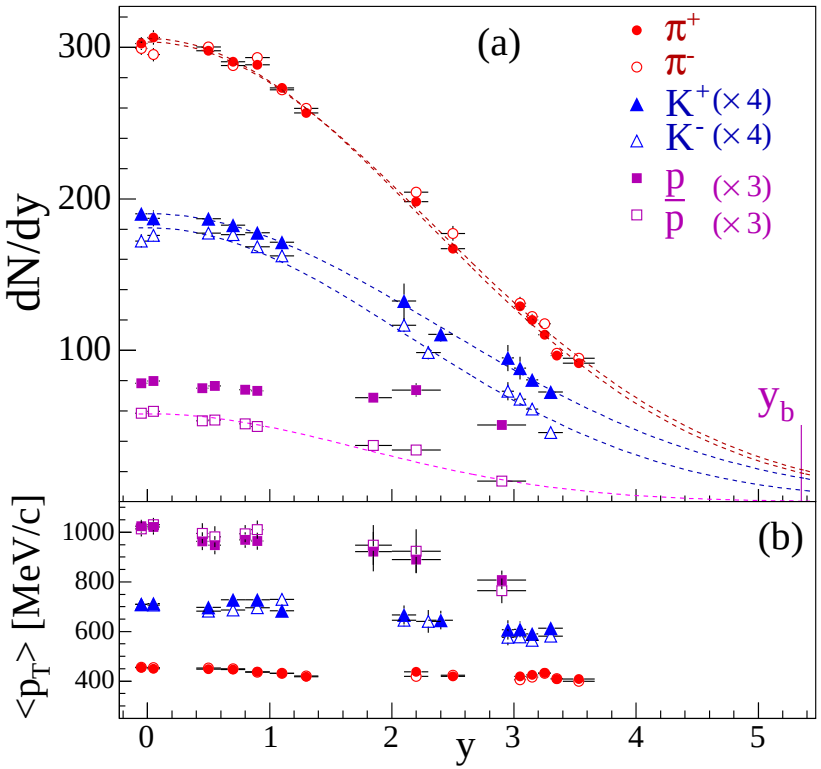

2.2.2 Kinematical variables: pseudorapidity

In the similar way one defines the **pseudorapidity** variable η, namely

$$\eta = \frac{1}{2} \ln \frac{(|\mathbf{p}|+p_{\parallel})}{(|\mathbf{p}|-p_{\parallel})} = \ln\left(\cot\frac{\theta}{2}\right) = -\ln\left(\tan\frac{\theta}{2}\right), \tag{8}$$

where θ is the **scattering angle**. In analogy to Eqs. (6) and (7) we have

$$|\mathbf{p}| = p_{\perp} \cosh\eta \tag{9}$$

and

$$p_{\parallel} = p_{\perp} \sinh\eta. \tag{10}$$

2.2.2 Kinematical variables: pseudorapidity

Pseudorapidity distributions of the charged particles measured by the PHOBOS Collaboration in Au+Au collisions at $\sqrt{s_{\mathrm{NN}}}$ = 130 GeV. The measurements were done for six different centrality classes (the latter will be defined precisely below).

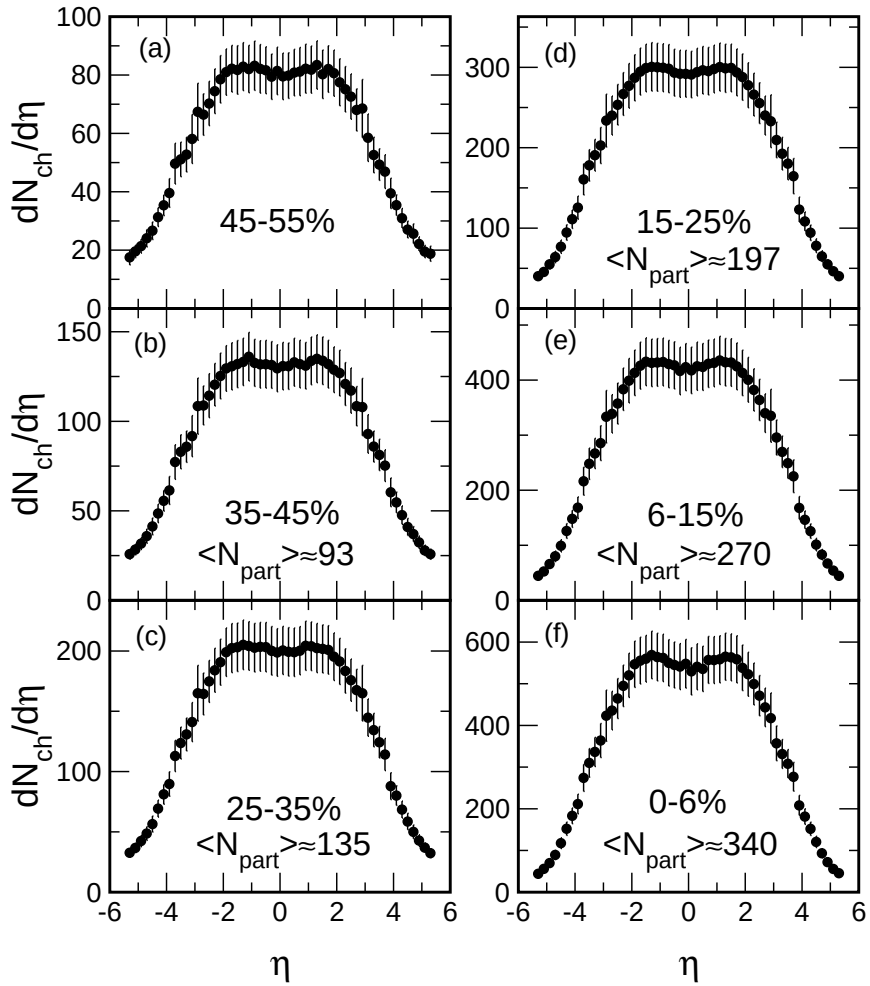

2.2.2 Kinematical variables: rapidity vs. pseudorapidity

In the limit $m \longrightarrow 0$, the rapidity and the pseudorapidity become equal. For finite masses the relations between the rapidity and the pseudorapidity are more complicated

$$y = \frac{1}{2} \ln \left[\frac{\sqrt{p_\perp^2 \cosh^2 \eta + m^2} + p_\perp \sinh \eta}{\sqrt{p_\perp^2 \cosh^2 \eta + m^2} - p_\perp \sinh \eta} \right], \tag{11}$$

$$\eta = \frac{1}{2} \ln \left[\frac{\sqrt{m_\perp^2 \cosh^2 y - m^2} + m_\perp \sinh y}{\sqrt{m_\perp^2 \cosh^2 y - m^2} - m_\perp \sinh y} \right]. \tag{12}$$

Equations (11) or (12) can be used to find a connection between the rapidity distribution of particles and the pseudorapidity distribution

$$\frac{dN}{d\eta\, d^2p_\perp} = \sqrt{1 - \frac{m^2}{m_\perp^2 \cosh^2 y}}\ \frac{dN}{dy\, d^2p_\perp} = \frac{|\mathbf{p}|}{E}\ \frac{dN}{dy\, d^2p_\perp}. \tag{13}$$

2.2.2 Kinematical variables: central rapidity region

In the center-of-mass frame, the region of the phase-space where $y \approx \eta \approx 0$ is called the **central rapidity region** or the **midrapidity region**. On the other hand, the regions corresponding to the initial rapidities of the projectile and target ($y \approx y_P$, $y \approx y_T$) are called the projectile and target **fragmentation regions**, respectively.

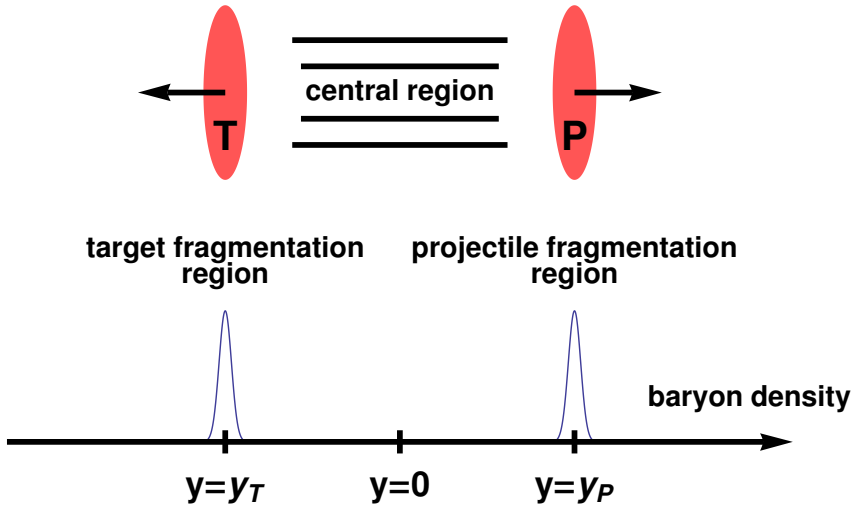

2.3 Centrality

W. Broniowski, WF, PRC 65, 024905 (2002)

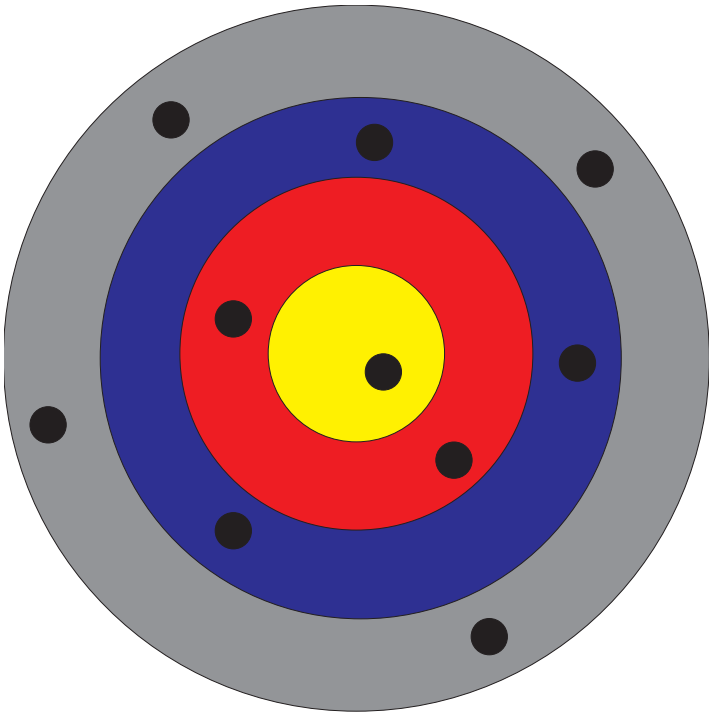

Archers shoot randomly at the target. The black dots describe their results. Knowing the rewards given to the archers we are able to conclude about the size of the bull's-eye of the target. Similarly, in the heavy-ion experiment we can make an estimate of the size of the overlapping region of two nuclei, if the number of the produced particles (a reward in this case) is a monotonic function of this size.

2.3 Centrality

Let $P(n)$ denote the probability of obtaining value n for multiplicity of produced particles, number of participants, number of binary collisions, ... **The centrality c is defined as the cumulant of $P(n)$**,

$$c(N) = \sum_{n=N}^{\infty} P(n). \tag{14}$$

A particular value of n may be collected from collisions with various impact parameters b',

$$c(N) = \sum_{n=N}^{\infty} \int_0^{\infty} \frac{2\pi b' db'}{\sigma_{\rm in}^{AB}} \rho(b') P(n|b'), \tag{15}$$

where $\rho(b')$ **is the probability of an event** (inelastic collision) at impact parameter b', and $P(n|b')$ **is the conditional probability of producing n provided the impact parameter is b'**. We have

$$\sum_{n=1}^{\infty} P(n|b') = 1, \tag{16}$$

and

$$\int_0^{\infty} 2\pi b' db' \rho(b') = \sigma_{\rm in}^{AB}. \tag{17}$$

2.3 Centrality

For large values of n we expect that $P(n|b') = \delta(n - \bar{n}(b'))$. In this case

$$\begin{aligned} c(N) &= \int_0^\infty dn\, \theta(n-N) \int_0^\infty \frac{2\pi b'\, db'}{\sigma_{\rm in}^{AB}} \rho(b') \delta(n - \bar{n}(b')) \\ &= \int_0^\infty \frac{2\pi b'\, db'}{\sigma_{\rm in}^{AB}} \rho(b') \theta(\bar{n}(b') - N). \end{aligned} \tag{18}$$

Since $\bar{n}(b')$ is a **monotonically decreasing function** of b', we have $\theta(\bar{n}(b') - N) = \theta(\bar{n}(b') - N(b)) = \theta(b(N) - b')$, where $\bar{n}(b) = N$, and

$$c(N) = \int_0^\infty \frac{2\pi b'\, db'}{\sigma_{\rm in}^{AB}} \rho(b') \theta(b(N) - b') = \int_0^{b(N)} \frac{2\pi b'\, db'}{\sigma_{\rm in}^{AB}} \rho(b'). \tag{19}$$

For impact parameters smaller than the nucleus radius, $\rho(b')$ is constant, and we get

$$c(N) \simeq \frac{\pi b^2(N)}{\sigma_{\rm in}^{AB}}. \tag{20}$$

More realistic approach is based on the Monte-Carlo simulations
W. Broniowski et al. **GLISSANDO 1 & 2**

2.4 Reaction plane

In particle as well as in nuclear physics it is practical to introduce a coordinate system, where the spatial z-axis is parallel to the beam of the accelerator, and where the impact vector **b** points in x-direction. The two axes, x and z, span the **reaction plane** of a given collision.

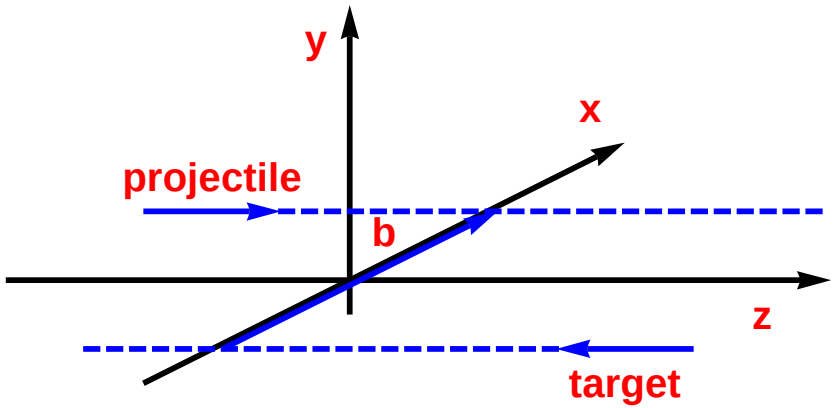

2.5 Collective flows

At present the extraction of the reaction (participant) plane is one aspect of the very advanced **flow analysis** of the collisions. In this type of the investigations one represents the momentum distribution of the produced particles in the form

$$\frac{dN}{dy d^2 p_\perp} = \frac{dN}{2\pi p_\perp dp_\perp dy}\left[1 + \sum_{k=1}^{\infty} 2v_k \cos\left(k(\phi_p - \Psi_k)\right)\right], \tag{21}$$

where Ψ_k is the reference angle defined by the condition $\langle \sin(k\Psi_k)\rangle = 0$, where the averaging is done over all particles in one event.

Until very recently it has been common to assume $\Psi_k = \Psi_{\rm RP}$.

Averaging of (21) over the azimuthal angle gives the transverse-momentum distribution (4). The coefficients v_k characterize the momentum anisotropy. The coefficient v_1 is called the **directed flow**, whereas the coefficient v_2 is called the **elliptic flow**. In general, the coefficients v_k are functions of rapidity and transverse momentum, $v_k = v_k(y, p_\perp)$, and in this form often called the kth harmonic **differential flow**.

2.5.1 Collective flows: directed flow

Schematic view of the directed flow observed at relativistic energies. For positive and large rapidities ($\mathrm{y} \sim \mathrm{y}_P$) the spectators are deflected towards positive values of x. For positive and small rapidities ($\mathrm{y} \geq 0$) the produced particles have negative v_1, hence they are deflected towards negative values of x.

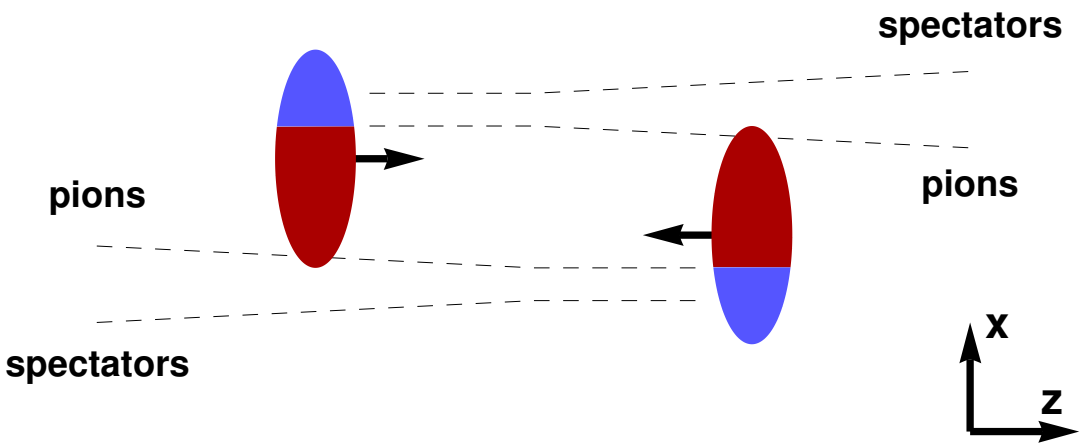

2.5.1 Collective flows: directed flow

The directed flow v_1 of charged particles as measured by STAR for three centralities in Au+Au collisions at $\sqrt{s_{\mathrm{NN}}}$ = 200 GeV. The arrows indicate v_1 for spectator neutrons, and their positions on the pseudorapidity axis correspond to the beam rapidity. The smaller window shows the midrapidity region in more detail. The figure includes also the PHOBOS results.

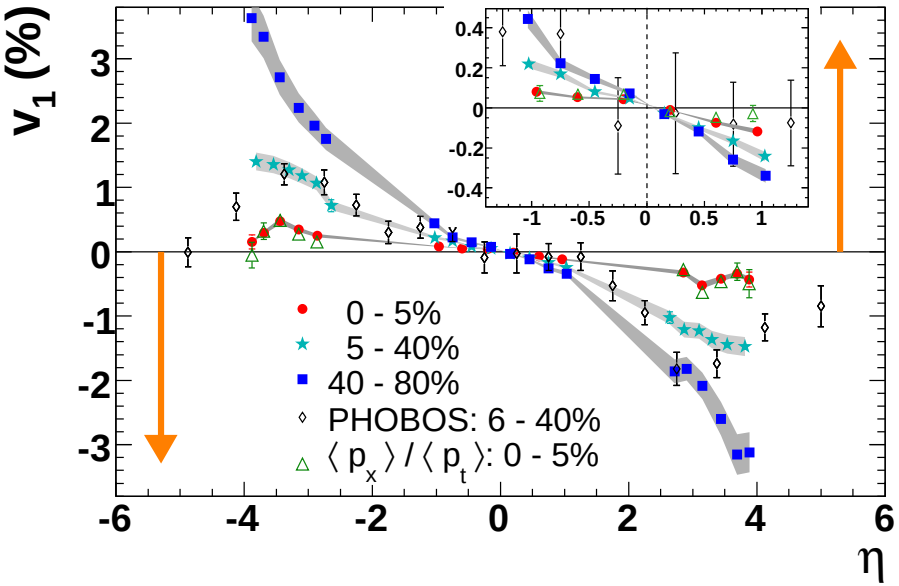

2.5.2 Collective flows: elliptic flow

In non-central collisions the region of the particle production has an almond shape in the transverse plane. Due to the interaction of the produced particles the spatial asymmetry leads to the azimuthal asymmetry of the momentum distributions. At ultra relativistic energies, the expansion is stronger in the reaction plane — the produced matter is not blocked by spectators.

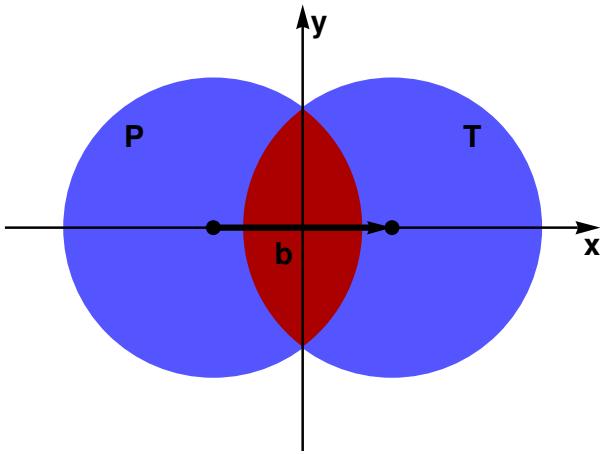

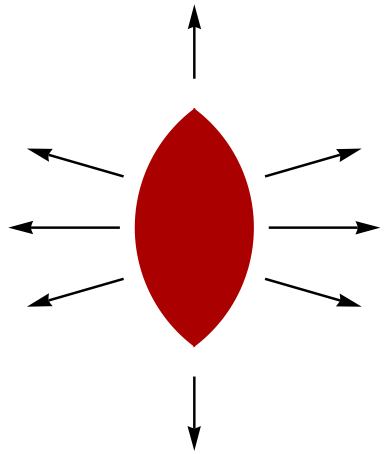

2.5.2 Collective flows: elliptic flow

Transverse-momentum dependence of the elliptic flow coefficient $v_2(\mathrm{y} = 0)$ as measured by PHENIX at $\sqrt{s_{\mathrm{NN}}}$ = 200 GeV for combined π^- and K^- (top) or π^+ and K^+(bottom), and compared with $\bar{p}$ (top) and p (bottom). The results for inclusive negative (top) and positive (bottom) charged particle distributions are plotted as open squares. From left to right, the three different centrality selections are shown.

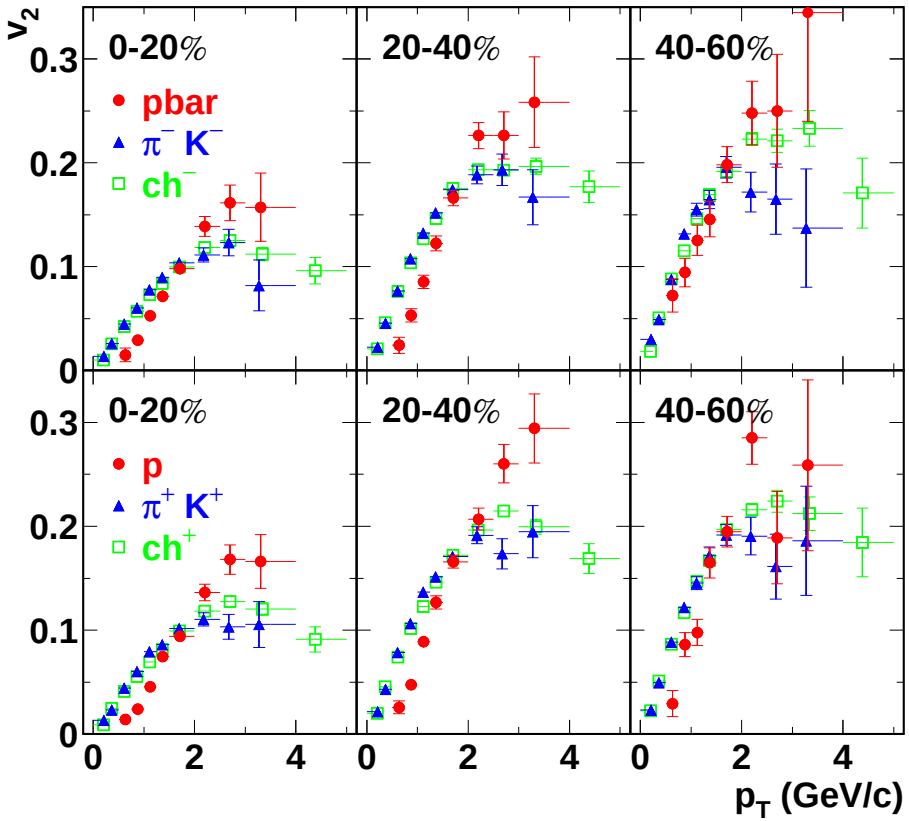

2.5.2 Collective flows: harmonic flows from the LHC

NEWS from the LHC: higher-order harmonic flows have been measured!

Higher order flow harmonics

- The p_T-dependence of v_2-v_6 for several centrality selections
- EP is calculated in full FCal (without separation for positive and negative hemisphers) to improve resolution for higher harmonics
- Similar p_T-dependence for all harmonics
- v_n generally decreases for larger n, except in the most central events:
  v_3 dominates in p_T range ~2-7GeV
  $v_4 > v_2$ in p_T range ~3-5GeV

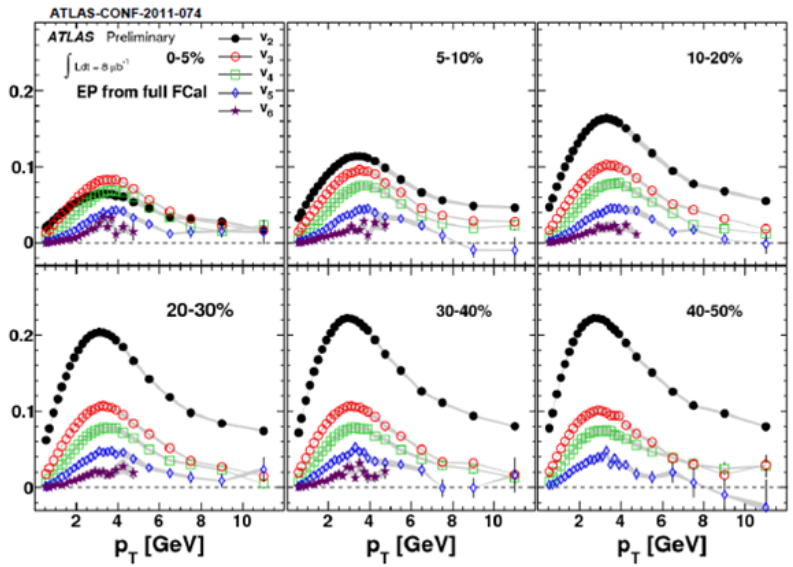

11

D. Derendarz, ATLAS, talk at SQM2011, Cracow

2.6 Stopping and transparency

The relativistic heavy-ion collisions can proceed in two different ways. In the collisions with large **stopping power** the baryons from the colliding nuclei are stopped in the middle of the reaction zone, and a dense baryon-rich matter is produced at midrapidity. On the other hand, in the **transparent** collisions (negligible stopping) the initial baryons are not slowed down, and the two baryon-rich regions are separated from each other.

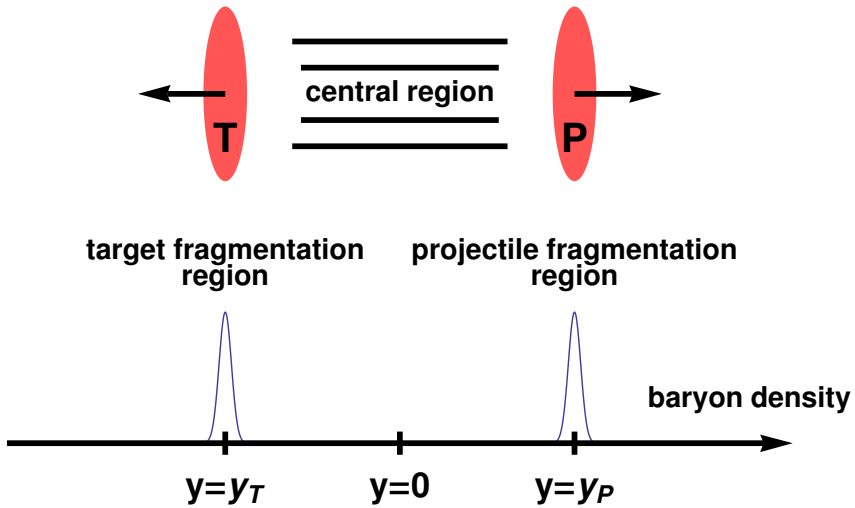

2.6 Stopping and transparency

The net-proton distributions measured in different experiments.

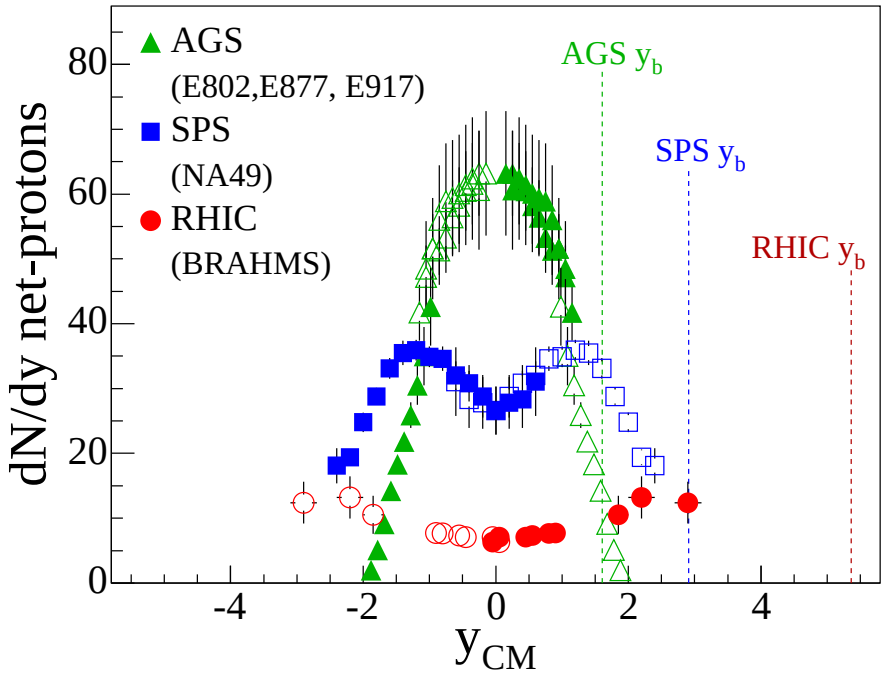

2.7 Boost invariance

Generally speaking, boost-invariance is the symmetry of the physical systems with respect to Lorentz boosts along the beam axis. It imposes special constraints on the form of the physical quantities.

For example, the thermodynamic functions used in the relativistic hydrodynamics, such as temperature, pressure, or the energy density, are Lorentz scalars. The boost-invariance in this cases means that they may depend only on the transverse coordinates and the longitudinal proper time $\tau = \sqrt{t^2 - z^2}$.

Similarly, the rapidity distribution dN/dy is boost-invariant if it is independent of rapidity.

2.7 Boost invariance:scalar field

From the formal point of view, a scalar field $\psi(x)$ has the following transformation rule

$$\psi(x) \to \psi'(x'), \qquad \psi'(x') = \psi(x), \tag{22}$$

where x, x' are spacetime coordinates connected by the Lorentz transformation L, namely $x' = Lx$. The scalar field is invariant under Lorentz boosts along the z axis if the transformed field in the new spacetime point x' coincides with the original field at that point,

$$\psi'(x') = \psi(x'). \tag{23}$$

Combining Eqs. (22) and (23), one obtains the constraint

$$\psi(x') = \psi(x), \tag{24}$$

which means that ψ may depend only on the transverse variables x, y and the longitudinal proper time $\tau = \sqrt{t^2 - z^2}$, as we have stated before.

2.7 Boost invariance: vector field

Schematic illustration of the rotational invariance of the vector field. If the vector field is rotationally invariant, as in panel **(a)**, the rotation of a vector yields the "new" vector placed in the "new" place that coincides with the "old" vector in the same "new" place. For example, the dashed arrow in **(b)**, after the rotation by $\pi/3$, coincides with the dashed vector in **(c)**. This property does not hold for the non-symmetric field in **(d)**. The rotation of the dashed vector in **(e)** by $\pi/3$ yields the the dashed vector in **(f)**, that does not agree with the old vector at that place.

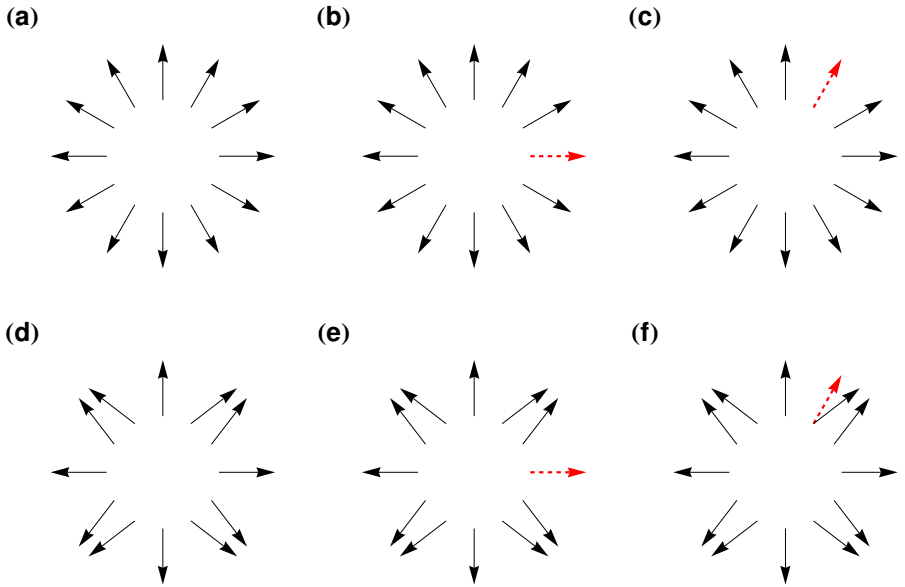

2.7 Boost invariance: vector field

It is also interesting to analyze the boost-invariant four-vector field. The general transformation rule in this case is

$$u^{\mu}(x) \to u'^{\mu}(x'), \qquad u'^{\mu}(x') = L^{\mu}{}_{\nu} u^{\nu}(x). \tag{25}$$

The boost-invariance demands again that the transformed "new" field u'^{μ} in the "new" spacetime point x' coincides with the original "old" field at this point

$$u'^{\mu}(x') = u^{\mu}(x'). \tag{26}$$

Equations (25) and (26) lead to the condition

$$u^{\mu}(x') = L^{\mu}{}_{\nu} u^{\nu}(x), \tag{27}$$

which states that the transformed boost-invariant field may be obtained by the simple substitution of the argument, $x \to x'$.

2.7 Boost invariance: four-velocity field

As an example we may consider the four-vector field which describes the hydrodynamic flow of matter produced in heavy-ion collisions. With the condition that the flow is zero for $z = 0$ one may check that the boost-invariant form of such a flow is

$$u^\mu = \gamma(1, v_x, v_y, v_z) = \bar{\gamma}(\tau, x, y)\,\frac{t}{\tau}\left(1, \frac{\tau}{t}\bar{v}_x(\tau, x, y), \frac{\tau}{t}\bar{v}_y(\tau, x, y), \frac{z}{t}\right), \tag{28}$$

where, to fulfill the normalization condition for the four-velocity, $u^\mu u_\mu = 1$, one assumes

$$\bar{\gamma} = \frac{1}{\sqrt{1 - \bar{v}_x^2 - \bar{v}_y^2}}. \tag{29}$$

As may be inferred from (28), the functions $\bar{v}_x$, $\bar{v}_y$, and $\bar{\gamma}$ are the transverse components of the fluid velocity and the corresponding Lorentz gamma factor, all determined in the plane $z = 0$ (where also $\tau = t$). The longitudinal flow has the scaling form

$$v_z = \frac{z}{t}. \tag{30}$$

EXERCISES

Exercise

1. Natural system of units.
Given the Planck constant $\hbar = 6.58 \cdot 10^{-22}$ *MeV s, the speed of light in vacuum* $c = 2.998 \cdot 10^{8}$ *m/s, and the Boltzmann constant* $k_{\mathrm{B}} = 1.38 \cdot 10^{-16}$ *erg/K (1 eV = 1.6* $\cdot 10^{-12}$ *erg).* **i)** *What length is equivalent to 1 GeV in the natural system of units where* $\hbar = c = k_{\mathrm{B}} = 1$*. Express your result in fm.* **ii)** *What temperature (in K) is equivalent to 100 MeV?* **iii)** *Change the standard unit used for the cross sections, 1 milibarn = 1 mb =* 10^{-31} m^2*, to* fm^2*.*

Answers:

$$1\ GeV = 5.07\ fm^{-1}\,, \tag{31}$$

$$100\ MeV = 116 \cdot 10^{10}\ K\,, \tag{32}$$

$$10\ mb = 1\ fm^2\,. \tag{33}$$

Exercise

2. Energy density of normal nuclear matter.
Calculate the energy density of normal nuclear matter.

Answer: The easiest way is to use the value of the nuclear saturation density $\rho_0 = 0.17\ fm^{-3}$ *and to multiply it by the nucleon mass* $m_{\mathrm{N}} = 940\ MeV$. *This gives*

$$\varepsilon_0 \approx 0.16\ GeV/fm^3\ . \tag{34}$$

Find other ways of making this estimate.

Exercise

3. Kinetic energy of a truck.
The weight of a truck is 10 tons and it is moving at a speed of 100 km/h. Calculate its kinetic energy in eV.

Exercise

4. Participants and spectators.
i) *Calculate the number of the participant nucleons in a central collision of the two nuclei characterized by the atomic numbers A and B (the impact parameter is exactly zero, $b = 0$). Assume that the nuclei have sharp surfaces and their density distribution is uniform and equal to the saturation density $\rho_0 = 0.17/fm^3$.* **ii)** *Find the numerical value of $N_{\rm part}$ for the central S+Au reaction.*

Answers:
We assume $B \leq A$ and use the following notation: $R = 1.12A^{1/3}$, $r = 1.12B^{1/3}$, $H = \sqrt{R^2 - r^2}$, and $h = R - H$. Simple geometric considerations, see figure, lead to the formula

$$N_{\rm part} = B + \left[2\pi r^2 H + \frac{2}{3}\pi h^2(3R - h)\right]\rho_0. \tag{35}$$

For $A = 197$ and $B = 32$ one finds $N_{\rm part} = 113$.

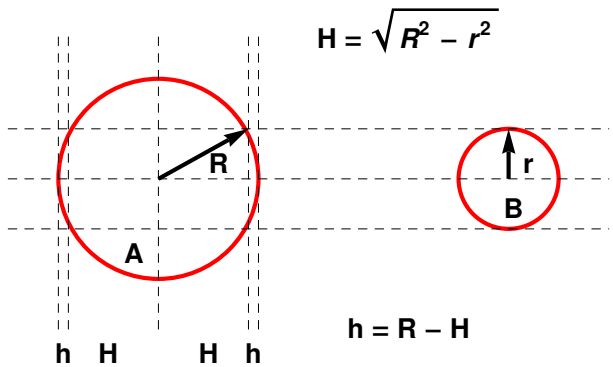

Exercise

5. Transverse-momentum spectra.
i) *For the exponential distribution function given by (4) show that the average transverse mass, $\langle m_\perp \rangle$, and the average transverse momentum, $\langle p_\perp \rangle$, are given by the expressions,*

$$\langle m_\perp \rangle = \frac{2\lambda^2 + 2\lambda m + m^2}{\lambda + m}, \tag{36}$$

$$\langle p_\perp \rangle = \frac{m^2 K_2(m/\lambda)}{\lambda + m} e^{m/\lambda}, \tag{37}$$

where m is the particle's mass. Hint: In the calculation of the average transverse momentum use the definition of the modified Bessel function of the second kind (next page). **ii)** *In the limit $m/\lambda \ll 1$ show that*

$$\langle m_\perp \rangle \approx 2\lambda + \frac{m^2}{\lambda}, \langle p_\perp \rangle \approx 2\lambda + \frac{m^2}{2\lambda},$$

which leads to $\langle m_\perp \rangle - \langle p_\perp \rangle \approx m^2/(2\lambda)$. Hint: In (37) use the asymptotic expansion for K_2 (next page).

The modified Bessel functions of the second kind (McDonald functions):

$$K_n(x) = \frac{2^n n!}{(2n)!} x^{-n} \int_x^\infty d\tau \, \left(\tau^2 - x^2\right)^{n-1/2} e^{-\tau}. \tag{38}$$

By the integration by parts one may show that (38) is equivalent to

$$K_n(x) \quad = \quad \frac{2^{n-1}\,(n-1)!}{(2n-2)!} x^{-n} \int_x^\infty d\tau \, \left(\tau^2 - x^2\right)^{n-3/2} \tau \, e^{-\tau}. \tag{39}$$

One may also check that

$$K_{n+1}(x) = \frac{x^n}{(2n-1)!!} \int_0^\infty e^{-x\,\mathrm{cosh}y} \mathrm{sinh}^{2n} y \,\mathrm{cosh}y \, dy, \tag{40}$$

which in the special cases gives

$$K_1(x) = \frac{1}{2} \int_{-\infty}^\infty e^{-x\,\mathrm{cosh}y} \,\mathrm{cosh}y \, dy \quad K_0(x) = \frac{1}{2} \int_{-\infty}^\infty e^{-x\,\mathrm{cosh}y} \, dy. \tag{41}$$

The series expansions of the modified Bessel functions $K_n(x)$ for $x \to 0$ and for $n = 1, 2, 3, 4$ are given by the formulas

$$\begin{aligned} K_1(x) &= \frac{1}{x} + O(x^1), \\ K_2(x) &= \frac{2}{x^2} - \frac{1}{2} + O(x^2), \\ K_3(x) &= \frac{8}{x^3} - \frac{1}{x} + \frac{x}{8} + O(x^3), \\ K_4(x) &= \frac{48}{x^4} - \frac{4}{x^2} + \frac{1}{4} - \frac{x^2}{48} + O(x^4). \end{aligned} \tag{42}$$

The asymptotic expansion of the modified Bessel function $K_n(x)$ for $x \to \infty$ has the generic form

$$K_n(x) = e^{-x} \left(\sqrt{\frac{\pi}{2x}} + O\left(x^{-\frac{3}{2}}\right) \right). \tag{43}$$

Exercise

6. Properties of rapidity.
i) *Calculate the rapidities of the projectile nuclei in the SPS fixed-target experiments with the beam energy of 60 and 200 GeV per nucleon.* **ii)** *Prove that rapidities are additive under Lorentz boosts along the beam axis.* **iii)** *Show that for a high-energy particle one can measure independently its rapidity and longitudinal position.*

Exercise

7. Properties of pseudorapidity.
Using elementary trigonometric identities derive

$$\eta = \frac{1}{2} \ln \frac{(|\mathbf{p}| + p_{\parallel})}{(|\mathbf{p}| - p_{\parallel})} = \ln \left(\cot \frac{\theta}{2} \right) = - \ln \left(\tan \frac{\theta}{2} \right), \tag{44}$$

$$\sin \theta = \frac{1}{\cosh \eta}. \tag{45}$$

Exercise

8. Boost-invariance.
Show that the longitudinal velocity of the form

$$v_z = \frac{Az - Bt}{At - Bz}, \tag{46}$$

where A and B are constants, is boost-invariant. Hint: Calculate the corresponding four-vector $u^\mu = \gamma(1, v_z)$*. Apply the longitudinal Lorentz boost and check that* u^μ *is boost-invariant .*

Exercise

9. Thickness functions.
i) *Show that the nucleon-nucleus thickness function for the sharp-cutoff baryon distribution and* $t(\mathbf{b}) = \delta^{(2)}(\mathbf{b})$ *is given by the formula*

$$T_A(b) = \frac{3\sqrt{R^2 - b^2}}{2\pi R^3}\theta(R - b). \tag{47}$$

ii) *Calculate the nucleon-nucleus thickness function for the Gaussian baryon distribution*

$$\rho_A(\mathbf{s}_A, z_A) = \frac{1}{(2\pi)^{3/2}\sigma_A^3}\exp\left(-\frac{\mathbf{s}_A^2 + z_A^2}{2\sigma_A^2}\right). \tag{48}$$

iii) *Use the result of point* **ii)** *to show that for the gaussian baryon distributions the nucleus-nucleus thickness function is a Gaussian characterized by the width*

$$\sigma_{AB} = \sqrt{\sigma_A^2 + \sigma_B^2}. \tag{49}$$

Exercise

10. EOS of the weakly-interacting quark-gluon plasma.
Calculate the energy density $\varepsilon = \varepsilon(T, \mu)$ of the weakly-interacting quark-gluon plasma consisting of massless partons. Hint: Treat gluons and quarks as an ideal Bose-Einstein and Fermi-Dirac gas, respectively.